Nanoscale

Accepted Manuscript

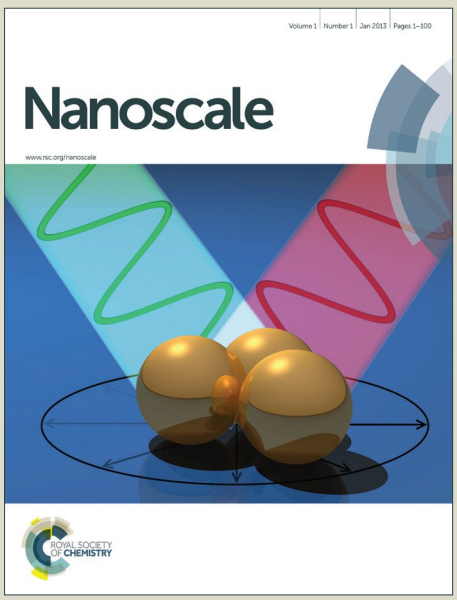

ROYAL SOCIETY OF CHEMISTRY

www.rsc.org/nanoscale

Journal Name

RSCPublishing

COMMUNICATION

Sulfur-Infiltrated Graphene-Backboned Mesoporous Carbon Nanosheets with Conductive Polymer Coating for Long-life Lithium-Sulfur Batteries

Cite this: DOI: 10.1039/xoxxoooooox

Received ooth January 2012,
Accepted ooth January 2012

DOI: 10.1039/xoxxoooooox

www.rsc.org/

Yanfeng Dong, Shaohong Liu, Zhiyu Wang,* Yang Liu, Zongbin Zhao,* Jieshan Qiu *

Sandwich-type, two-dimensional hybrid nanosheets were fabricated by the infiltration of nanosized sulfur into graphene-backboned mesoporous carbon with PPy nanocoating. They exhibit high reversible capacity for as long as 400 cycles with ultraslow decay rate of 0.05% per cycle at high rate of 1-3 C due to efficient immobilization of polysulfides.

Lithium-sulfur (Li-S) batteries are very appealing power source of electric vehicles in virtue of very high theoretical energy density of up to 2567 W h kg^{-1}.[1, 2] Other features like low cost, nontoxicity and natural abundance of sulfur bring extra benefit to their market potential. Despite the great promise, the commercialization of Li-S batteries is greatly hindered by several critical difficulties arose from complex sulfur chemistry:[2-4] i) low utilization of sulfur cathode due to the insulating nature of sulfur (5×10^{-30} S cm^{-1}) and solid-state discharge products; ii) highly soluble polysulfide intermediates causes rapid sulfur loss, notorious shuttle effect and over charge; iii) dramatic volume expansion (over 80 %) of sulfur during cycling reduces the electrode stability. Overall, the coupled chemical and mechanical degradation, as well as sluggish kinetics, leads to poor operational performance of Li-S batteries, including the low capacity, short lifespan, fast self-discharge and inferior routine efficiency.[5-7]

Coupling sulfur to porous carbon has been regarded as the major approach to partly overcome the drawbacks of sulfur cathode.[8-23] Commonly, porous carbon hosts play dual roles in the enhancement of cell performance: the carbon matrix greatly facilitates the electron transport across the electrode and cushions the volume change of sulfur upon cycling; while the porous structure effectively restrains the sulfur and retards polysulfide diffusion. As smaller pores usually exhibit higher energy barrier for polysulfide diffusion, various mesoporous carbon with tuneable nanoporosity have been exploited to achieve efficient entrapment of sulfur species.[16-19] However, the physical barrier provided by open nanopores can only slow down the escape of polysulfide in a short while due to weak interaction between nonpolar carbon and highly polar polysulfides.[9-22, 24] Coating mesoporous carbon with a thin layer of conducting polymer with electronic and ionic conductivity such as PEO, PEDOT:PSS and polyaniline has proven being effective to largely prevent the sulfur from loss.[16, 25, 26] Though the discharge capacity is improved, the cycling performance and rate capability of the cell is still hampered by limited conductivity and large size of mesoporous carbon particles. Engineering nanostructured mesoporous carbon with reduced pathway for ionic diffusion and electronic transport has been known as one effective way towards high-performance sulfur/carbon cathode. For example, the graphene, an one-atom-thick two dimensional (2D) carbon layer, has been employed to direct the growth of layered porous carbon with high conductivity, large surface area and good mechanical flexibility.[14, 15, 27] The synergistic effect of graphene and nanostructured mesoporous carbon could enhance the cycling life of Li-S batteries to some extent (up to 100 cycles). Nevertheless, the long-term cycling performance of such materials, especially at high current rate, is still a concern for practical applications.

Herein, we report an efficient approach towards long-life sulfur cathode by rational integration of sulfur-infiltrated mesoporous carbon, graphene and conducting polymer coating into a sandwich-type hybrid nanosheet. This architecture is designed with several specific goals in mind: i) the graphene guides the growth of mesoporous carbon nanosheet and acts as nanoscale current collector in individual sheet; ii) 2D thin nanosheet with large surface area facilitates sulfur penetration and ionic diffusion; iii) mesoporous carbon serves as sulfur reservoir and nanoreactor for complete redox process; iv) the outmost nanocoating by elastic conducting polymer prevents the polysulfides from escape and strengthen the entire sheet. As the proof-of-concept demonstration, sulfur-infiltrated graphene-backboned mesoporous carbon nanosheets with polypyrrole (PPy) coating (denoted as GCS@PPy) are successfully synthesized as the cathode materials in Li-S batteries, exhibiting high reversible capacity and long lifespan of 400 cycles with ultraslow decay rate of 0.05% per cycle at high rate of 1-3 C in favor of enhanced electrode kinetics and stability.

The synthetic strategy of GCS@PPy nanosheets is illustrated in Scheme 1. Firstly, graphene-backboned mesoporous carbon (GC) nanosheets are fabricated by nanocasting against graphene-based mesoporous SiO_2 nanosheets with sucrose as carbon precursor. Scanning electron microscopy (SEM) and transmission electron microscopy (TEM) analysis reveals that the GC sheets possess crumpled sheet-like structure with specific surface area of as high as

904 m^2 g^{-1} and large pore volume of 1.18 cm^3 g^{-1} (Fig. S1 and Fig. S2). Sufficient porosity of GC sheets provides the feasibility for efficient sequestration and adsorption of high-content sulfur via the melting-diffusion of liquid sulfur at 155 ^oC. After sulfur infiltration, the resultant nanohybrids (denoted as GCS) inherit the nanosheet morphology of GC with homogenous distribution of sulfur in the structure, as shown in Fig. 1a-c. No sulfur residues appear on the external surface of GCS sheets. However, we fail in obtaining a high-resolution TEM image of nanosized sulfur because they sublimate very fast under electron beam irradiation. Finally, PPy nanocoating is carried out by precisely controlled polymerization of pyrrole around GCS nanosheets in the presence of ammonium peroxydisulfate (APS) at room temperature. The as-prepared GCS@PPy nanohybrids well retain the nanosheet structure without change of the sulfur distribution (Fig. 1d-f). The overall content of sulfur in this sample is measured to be ca. 64 wt. % by thermogravimetric analysis (TGA), as shown in Fig. S3. The content of PPy, graphene and mesoporous carbon in the sample is estimated to be ca. 11 wt. %, 8.8 wt.% and 16.2 wt.% by measuring the difference in sample weight before and after loading PPy or mesoporous carbon, respectively.

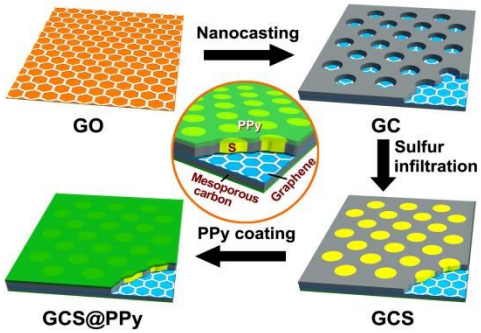

Scheme 1. Schematic illustration of the synthesis procedure of GCS@PPy hybrid nanosheets.

Structural characteristics of GCS and GCS@PPy nanosheets are identified by X-ray powder diffraction (XRD), as shown in Fig. 2a. For both samples, all the pronounced peaks can be assigned to orthorhombic sulfur (JCPDS No: 08-0427) except the broad one from mesoporous carbon and graphene between 20-30°.[14] Despite the high content, the intensity of sulfur peaks in GCS and GCS@PPy samples is largely reduced as compared to that of sulfur powder, implying the even dispersion of nanosized sulfur within the hybrid nanosheets.[14, 15, 28] In Raman spectra, the absence of fingerprint peaks of sulfur in the range of 100-500 cm^{-1}, which are related to S-S bond vibration in sulfur crystal, further reveals that sulfur is dispersed in both samples without long-range ordering (Fig. 2b).[29, 30] Owing to infrared inactivity of sulfur, GCS sheets exhibit few signals in Fourier transform-infrared spectroscopy (FTIR). However, the rise of new peaks after PPy coating strongly confirms the presence of PPy layer around GCS sheets (Fig. 2c). Specifically, the pronounced adsorption bands at 1544 and 1470 cm^{-1} can be ascribed to fundamental stretching vibrations of C–N and C–C bonds in pyrrole ring, respectively.[31] The broad band at 1300 and 1040 cm^{-1} is associated with the C−N stretching and C−H deformation vibrations, respectively. The strong peaks near 1175 cm^{-1} represent the doping state of PPy.[32] The successful loading of sulfur is depicted by the S 2p spectrum of X-ray photoelectron spectroscopy (XPS), as characterized by the S $2p_{3/2}$ and $2p_{1/2}$ doublet with an energy separation of 1.4 eV and intensity ratio of about 2:1 (Fig. 2d).[22] The binding energy of S $2p_{3/2}$ peak is 163.6 eV, which is slightly lower than that of elemental sulfur (164.0 eV), revealing the possible presence of C-S species.[22, 33] The peak at 167.0-171.0 eV is due to the sulfate species formed by sulfur oxidation in air and residual ammonium peroxydisulfate.[10] In the range of XPS sensitivity, only carbon, nitrogen, oxygen and sulfur are detected in the survey scan (Fig. S4), thus excluding the presence of other impurities.

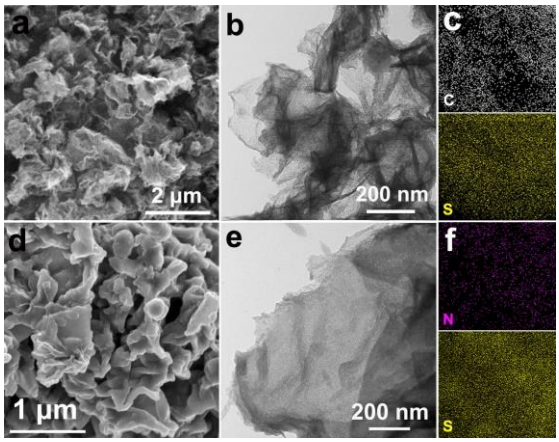

Fig. 1. (a) SEM and (b) TEM image of GCS nanosheets; (c) elemental mapping showing uniform distribution of carbon and sulfur in GCS sheets; (d) SEM and (e) TEM image of GCS@PPy nanosheets; (f) elemental mapping indicating homogenous presence of nitrogen and sulfur in GCS@PPy sheets.

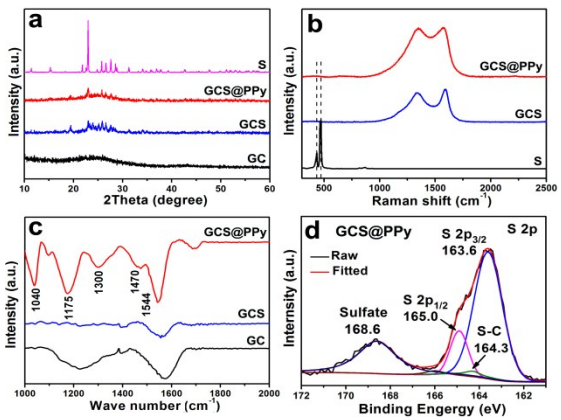

Fig. 2. (a) XRD patterns of GC, GCS, GCS@PPy nanosheets and sulfur powder; (b) Raman spectra of GCS, GCS@PPy sheets and sulfur powder; (c) FTIR spectra of GC, GCS and GCS@PPy sheets; (d) S 2p XPS spectrum of GCS@PPy nanosheets.

Electrochemical route of GCS@PPy electrode towards lithium storage is monitored by cyclic voltammetry (CV) analysis within a cut-off voltage window of 1.5-3.0 V at a scan rate of 0.1 mV s^{-1}, as shown in Fig. 3a. In the first cycle, two cathodic peaks are observed at ca. 2.32 and 2.05 V due to multistep reduction of elemental sulfur with lithium in organic electrolyte. Specifically, the peak at 2.32 V is associated with the solid-to-liquid (from S_8 to high-order Li_2S_x, $4 \leq x \leq 8$) phase transition while the one at 2.05 V is due to further reduction of soluble polysulfides to solid-state Li_2S/Li_2S_2.[9, 11, 34] The anodic peak at 2.37 V is the result of the formation of lithium polysulfides, which proceeds until the S_8 ring is restored at 2.42 V.[35, 36] The CV curves at subsequent cycles show good reproducibility with overlapping of all the peaks, suggesting good reversibility of multistep reactions.

Fig. 3b shows representative discharge/charge voltage profiles of GCS@PPy electrode at a current rate of 0.5 C (1 C = 1672 mA g^{-1}) in the voltage window of 1.5-3.0 V. Consistent with literature reports and above CV analysis, typical two-plateau behavior is observed for the

formation of long-chain polysulfides (high plateau at 2.35 V) and low-order (low flat plateau at 2.0 V) lithium sulfides during discharging.[7, 14] High initial discharge and charge capacity of 935 mAh g^{-1} and 873 mAh g^{-1} is delivered at the first cycle, respectively. The irreversible capacity loss of approximately 6.6 % is mainly attributed to initial irreversible processes such as the trapping of some lithium in polymer and carbon matrix, leading to an initial Coulombic efficiency of beyond 100 %. Since graphene and mesoporous carbon is electrochemically inert in the voltage region tested, they contribute few to total capacities.[7] The capacity from PPy is likewise negligible in the electrochemical window used (2.5-4.0 V). From the second cycle onwards, GCS@PPy electrodes exhibit stable capacity retention of over 90 % for 100 cycles, combined with a stabilized Coulombic efficiency of as high as 94 % (Fig. 3c). In a vast contrast, the electrodes consisting of GCS sheets without PPy coating, graphene-sulfur composite with (GS@PPy, 62 wt.% S) or without PPy coating (GS, 64 wt.% S) and mesoporous carbon-sulfur composite with PPy coating (CS@PPy, 65 wt.% S) udergo much faster capacity decay to ca. 450 mAh g^{-1} after 100 cycles under identical conditions, rendering poor suppression of polysulfide dissolution.

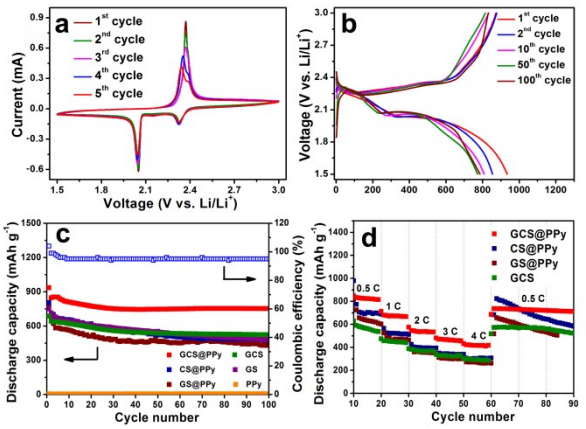

Fig. 3. (a) CV curves of GCS@PPy electrode at a scan rate of 0.1 mV s^{-1}; (b) discharge/charge voltage profiles of GCS@PPy electrodes at 0.5 C; (c) cycling capability and Coulombic efficiency of the electrodes composed of GCS@PPy, CS@PPy, GS@PPy, GCS, GS or PPy at 0.5 C; (d) rate capability of the electrodes composed of GCS@PPy, CS@PPy, GS@PPy or GCS at varied current rates. All these tests were conducted in the voltage window of 1.5-3.0 V.

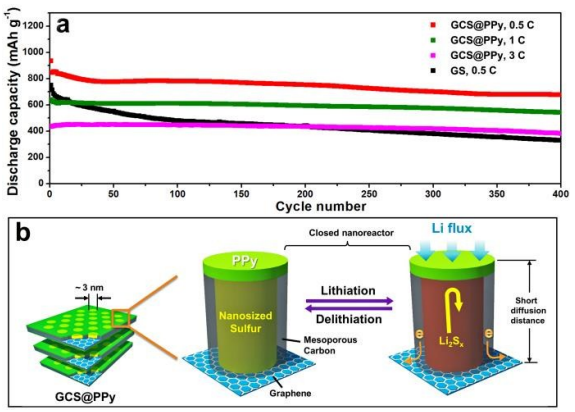

Fig. 4. (a) Long-term cycling stability of GCS@PPy electrodes at current rates of 0.5 C, 1 C and 3 C. Cycling curves of GS electrode at 0.5 C is also displayed as the comparison; (b) schematic illustration of structural merits of GCS@PPy hybrid nanosheets towards lithium storage, where 2D nanosheet structure facilitates sulfur loading and better diffusion kinetics, mesoporous carbon with nanoproosity act as sulfur reservoir and nanoreactor for redox process, graphene serves as nanoscale current collector in individual sheet for rapid electron transport and PPy coating prevents the discharge products from escape.

Furthermore, GCS@PPy electrodes also show greatly improved cycling response to continuously varying current rate despite that sulfur cathodes are generally observed to suffer from sluggish kinetics and poor conductivity, as shown in Fig. 3d. At high current rate of 0.5, 1, 2, 3 and 4 C, the electrode delivers the capacities of 830, 680, 550, 470 and 430 mAh g^{-1}, respectively. After deep cycling at 4 C, stable high capacity of 740 mAh g^{-1} can still be retained for repeated cycles after abruptly switching the current rate back to 0.5 C (Fig. 3d), showing robust structure of the electrode. For the electrodes composed of GCS, GS@PPy and CS@PPy, however, they exhibit much lower capacities of 580-710, 460-530, 360-400, 320 and 280 mAh g^{-1} at the current rate of 0.5, 1, 2, 3 and 4 C. Long-term cycling tests further reveal that GCS@PPy electrodes could exhibit stable capacity retention of over 80 % for as long as 400 cycles at high current rate of up to 3 C, corresponding to a ultraslow decay rate of 0.05% per cycle (Fig. 4a). Such a remarkable performance is superior to that of GS and most reported carbon-sulfur nanocomposites, of which the capacities fades rapidly in short term upon cycling under such high rates.[10, 21, 24, 30, 35, 37-42]

Superior performance of GCS@PPy sample is mainly attributed to the unique design of sandwich-type hybrid nanosheet and synergistic effect of each component in the structure, as schematically illustrated in Fig. 4b. Graphene acts as the shape-directing agent for the growth of mesoporous carbon nanosheet with large surface area, highly developed porosity but extremely reduced thickness. This feature not only benefits the sulfur penetration, but also affords sufficient electrolyte-electrode interface and short diffusion distance for rapid diffusion of electrolyte and lithium ions.[20, 43-45] More importantly, they could work as nanoscale current collectors to allow fast electron transport across each sheet, thereby reducing the electrically isolated volume in sulfur cathode. Electrochemical impedance spectroscopy (EIS) reveals the largely reduced charge-transfer resistance in GCS@PPy electrode, as characterized by much smaller diameter of the semicircle at high-frequency region than that of their counterparts without graphene involved (Fig. S5). On graphene, the mesoporous carbon have narrow pore size distribution centered at ca. 3 nm (Fig. S2). The presence of these nanopores enables the homogenous entrapment of nanosized sulfur within the hybrid nanosheets (see XRD and Raman analysis), and partially increases the energy barrier of polysulfides diffusion into the electrolyte.[12] Thus the electrochemical accessibility and utilization of sulfur could be greatly enhanced during cycling. Furthermore, the outmost continuous PPy nanocoating around the overall architecture not only serve as a buffering layer to cushion the internal strain associated with lithium uptaking, but improve the long-term stability of the hybrid nanosheets by efficiently sealing the polysulfides and solid-state Li_2S/Li_2S_2 inside the nanosheets. In this case, numerous closed nanoreactors could be generated in the hybrid nanosheets to achieve more efficient redox process and better electrode stability. To confirm this, the cells using different electrodes are discharged to 2.0 V and then disassembled for observation. For the cell with GS and GCS electrode, a thick layer of polysulfides with yellowish-brown color are deposited on the separators; whereas on the separator detached from the cell with GCS@PPy electrode, the polysulfide layer is much thinner with significantly lightened color (Fig. S6). Apparently, the unique design of GCS@PPy structure can efficiently reduce the concentration of polysulfides in electrolyte for better electrochemical performance. The robustness of GCS@PPy nanosheets towards lithium storage is evidenced by microscopy and

elemental mapping analysis, which reveals that homogeneous distribution of sulfur and nitrogen in these sheets can be well maintained even after 400 deep cycles without detachment or aggregation (Fig. S7). Additionally, the binding capability of PPy to discharge products via π-σ coordination between the heteroatoms with lone electron pairs (e.g., N) and lithium atom may also help to minimize the sulfur loss and electrode failure.[26, 46] Without graphene or mesoporous carbon involved, the electrodes exhibit much lower capacity, fast capacity fading and sluggish rate capability under identical conditions due to poor conductivity, inefficient utilization and immobilization of sulfur.

Conclusions

In summary, we have demonstrated the efficient entrapment of sulfur in sandwich-type 2D hybrid nanosheets consisting of graphene-backboned mesoporous carbon with PPy nanocoating. When evaluated as the cathode materials in Li-S batteries, they exhibit high durability of 400 cycles with stable capacity retention and greatly improved rate capability in virtue of unique hybrid nanostructure, where 2D nanosheet structure facilitates sulfur loading and better diffusion kinetics, mesoporous carbon with nanoporosity act as sulfur reservoir and nanoreactor for more complete redox process, graphene serves as nanoscale current collector in individual sheet for rapid electron transport and PPy coating prevents the discharge products from escape. We thus believe that this strategy of cathode design may shed some light on the fabrication of long-life Li-S batteries.

Acknowledgments

This work was partly supported by the National Natural Science Foundation of China (No. 51072028). Z. W. acknowledges the support from the Recruitment Program of Global Youth Experts (2014) and the start-up grant from Dalian University of Technology (No. 1000-852036).

Notes and references

Carbon Research Laboratory, Liaoning Key Lab for Energy Materials and Chemical Engineering, State Key Lab of Fine Chemicals, School of Chemical Engineering, Dalian University of Technology, Dalian 116023, China.

Email: zywang@ dlut.edu.cn; zbzhao@dlut.edu.cn; jqiu@dlut.edu.cn

Electronic Supplementary Information (ESI) available: Experimental details, BET, SEM, XPS and more electrochemical data. See DOI: 10.1039/c000000x/

1. P. G. Bruce, S. A. Freunberger, L. J. Hardwick and J. M. Tarascon, *Nat. Mater.*, 2012, 11, 19-29.
2. A. Manthiram, Y. Z. Fu, S. H. Chung, C. X. Zu and Y. S. Su, *Chem. Rev.*, 2014, 114, 11751–11787.
3. Y. X. Yin, S. Xin, Y. G. Guo and L. J. Wan, *Angew. Chem. Int. Ed.*, 2013, 52, 13186-13200.
4. J. Wang, Y. S. He and J. Yang, *Adv. Mater.*, 2015, 27, 569-575.
5. C. Huang, J. Xiao, Y. Shao, J. Zheng, W. D. Bennett, D. Lu, L. V. Saraf, M. Engelhard, L. Ji, J. Zhang, X. Li, G. L. Graff and J. Liu, *Nat. Commun.*, 2014, 5, 3015.
6. Y. S. Su and A. Manthiram, *Nat. Commun.*, 2012, 3, 1166.
7. Z. Wang, Y. Dong, H. Li, Z. Zhao, H. Bin Wu, C. Hao, S. Liu, J. Qiu and X. W. Lou, *Nat. Commun.*, 2014, 5, 5002.
8. S. Chen, X. Huang, H. Liu, B. Sun, W. Yeoh, K. Li, J. Zhang and G. Wang, *Adv. Energy Mater.*, 2014, 4, 1301761.
9. L. Ji, M. Rao, H. Zheng, L. Zhang, Y. Li, W. Duan, J. Guo, E. J. Cairns and Y. Zhang, *J. Am. Chem. Soc.*, 2011, 133, 18522-18525.
10. G. Zhou, L. C. Yin, D. W. Wang, L. Li, S. Pei, I. R. Gentle, F. Li and H. M. Cheng, *ACS Nano*, 2013, 7, 5367-5375.
11. M. Q. Zhao, Q. Zhang, J. Q. Huang, G. L. Tian, J. Q. Nie, H. J. Peng and F. Wei, *Nat. Commun.*, 2014, 5, 3410.
12. J. T. Lee, Y. Zhao, S. Thieme, H. Kim, M. Oschatz, L. Borchardt, A. Magasinski, W.-I. Cho, S. Kaskel and G. Yushin, *Adv. Mater.*, 2013, 25, 4573-4579.
13. Z. Li, L. Yuan, Z. Yi, Y. Sun, Y. Liu, Y. Jiang, Y. Shen, Y. Xin, Z. Zhang and Y. Huang, *Adv. Energy Mater.*, 2014, 4, 10.1002/aenm.201301473.
14. X. Yang, L. Zhang, F. Zhang, Y. Huang and Y. S. Chen, *ACS Nano*, 2014, 8, 5208-5215.
15. X. a. Chen, Z. Xiao, X. Ning, Z. Liu, Z. Yang, C. Zou, S. Wang, X. Chen, Y. Chen and S. Huang, *Adv. Energy Mater.*, 2014, 4, 1301988.
16. X. Ji, K. T. Lee and L. F. Nazar, *Nat. Mater.*, 2009, 8, 500-506.
17. J. Schuster, G. He, B. Mandlmeier, T. Yim, K. T. Lee, T. Bein and L. F. Nazar, *Angew. Chem. Int. Ed.*, 2012, 51, 3591-3595.
18. J. Wang, S. Y. Chew, Z. W. Zhao, S. Ashraf, D. Wexler, J. Chen, S. H. Ng, S. L. Chou and H. K. Liu, *Carbon*, 2008, 46, 229-235.
19. X. Li, Y. Cao, W. Qi, L. V. Saraf, J. Xiao, Z. Nie, J. Mietek, J. G. Zhang, B. Schwenzer and J. Liu, *J. Mater. Chem.*, 2011, 21, 16603-16610.
20. M. Q. Zhao, X. F. Liu, Q. Zhang, G. L. Tian, J. Q. Huang, W. C. Zhu and F. Wei, *ACS Nano*, 2012, 6, 10759-10769.
21. R. Elazari, G. Salitra, A. Garsuch, A. Panchenko and D. Aurbach, *Adv. Mater.*, 2011, 23, 5641-5644.
22. C. Zu and A. Manthiram, *Adv. Energy Mater.*, 2013, 3, 1008-1012.
23. S. Chen, X. Huang, B. Sun, J. Zhang, H. Liu and G. Wang, *J. Mater. Chem. A*, 2014, 2, 16199-16207.
24. C. Zhang, H. B. Wu, C. Yuan, Z. Guo and X. W. Lou, *Angew. Chem. Int. Ed.*, 2012, 51, 9592-9595.
25. G. C. Li, G. R. Li, S. H. Ye and X. P. Gao, *Adv. Energy Mater.*, 2012, 2, 1238-1245.
26. Y. Yang, G. Yu, J. J. Cha, H. Wu, M. Vosgueritchian, Y. Yao, Z. Bao and Y. Cui, *ACS Nano*, 2011, 5, 9187-9193.
27. X. Huang, B. Sun, K. Li, S. Chen and G. Wang, *J. Mater. Chem. A*, 2013, 1, 13484-13489.
28. J. Song, T. Xu, M. L. Gordin, P. Zhu, D. Lv, Y. B. Jiang, Y. Chen, Y. Duan and D. Wang, *Adv. Funct. Mater.*, 2014, 24, 1243-1250.
29. C. Zhang, W. Lv, W. Zhang, X. Zheng, M. B. Wu, W. Wei, Y. Tao, Z. Li and Q. H. Yang, *Adv. Energy Mater.*, 2014, 4, 10.1002/aenm.201301565.
30. R. Chen, T. Zhao, J. Lu, F. Wu, L. Li, J. Chen, G. Tan, Y. Ye and K. Amine, *Nano lett.*, 2013, 13, 4642-4649.
31. J. T. Zhang and X. S. Zhao, *J. Phys. Chem. C*, 2012, 116, 5420-5426.
32. S. Yang, C. Shen, Y. Liang, H. Tong, W. He, X. Shi, X. Zhang and H. J. Gao, *Nanoscale*, 2011, 3, 3277-3284.
33. L. Zhang, L. Ji, P. A. Glans, Y. Zhang, J. Zhu and J. Guo, *Phys. Chem. Phys. Chem.*, 2012, 14, 13670-13675.
34. Y. S. Su, Y. Fu, T. Cochell and A. Manthiram, *Nat. Commun.*, 2013, 4, 2985.
35. N. Jayaprakash, J. Shen, S. S. Moganty, A. Corona and L. A. Archer, *Angew. Chem. Int. Ed.*, 2011, 123, 6026-6030.

36. D. Aurbach, E. Pollak, R. Elazari and G. Salitra, *J. Electrochem. Soc.*, 2009, 156, A694-A702.
37. W. Zhou, H. Chen, Y. Yu, D. Wang, Z. Cui, F. J. DiSalvo and H. D. Abruña, *ACS Nano*, 2013, 7, 8801-8808.
38. H. Wang, Y. Yang, Y. Liang, J. T. Robinson, Y. Li, A. Jackson, Y. Cui and H. Dai, *Nano lett.*, 2011, 11, 2644-2647.
39. G. Zheng, Q. Zhang, J. J. Cha, Y. Yang, W. Li, Z. W. Seh and Y. Cui, *Nano lett.*, 2013, 13, 1265-1270.
40. S. Zheng, Y. Wen, Y. Zhu, Z. Han, J. Wang, J. Yang and C. Wang, *Adv. Energy Mater.*, 2014, 4, 10.1002/aenm.201400482.
41. Z. Lin, Z. Liu, W. Fu, N. J. Dudney and C. Liang, *Angew. Chem. Int. Ed.*, 2013, 52, 7460-7463.
42. S. Lu, Y. Cheng, X. Wu and J. Liu, *Nano lett.*, 2013, 13, 2485-2489.
43. Y. Yang, G. Zheng and Y. Cui, *Chem. Soc. Rev.*, 2013, 42, 3018-3032.
44. G. Xu, B. Ding, J. Pan, P. Nie, L. Shen and X. Zhang, *J. Mater. Chem. A*, 2014, 2, 12662-12676.
45. D. W. Wang, Q. Zeng, G. Zhou, L. C. Yin, F. Li, H. M. Cheng, L. R. Gentle and G. Q. Lu, *J. Mater. Chem. A*, 2013, 1, 9382-9394.
46. W. Li, Q. Zhang, G. Zheng, Z. W. Seh, H. Yao and Y. Cui, *Nano lett.*, 2013, 13, 5534-5540.